

SPECTRUM, LIFSHITZ TRANSITIONS AND ORBITAL CURRENT IN FRUSTRATED FERMIONIC LADDERS WITH A UNIFORM FLUX

Bachana Beradze^{1,2} and Alexander Nersesyan^{1,2,3}

¹ *The Andronikashvili Institute of Physics, 0177 Tbilisi, Georgia,*

² *Ilia State University, 0162 Tbilisi, Georgia and*

³ *The Abdus Salam International Centre for Theoretical Physics, 34151, Trieste, Italy*

(Dated: November 1, 2022)

Ultracold Fermi gases with synthetic gauge field represent an excellent platform to study the combined effect of lattice frustration and an effective magnetic flux close to one flux quantum per particle. The minimal theoretical model to accomplish this task is a system of spinless noninteracting fermions on a triangular two-chain flux ladder. In this paper we consider this model close to half-filling, with interchain hopping amplitudes alternating along the zigzag bonds of the ladder and being small. In such setting qualitative changes in the ground state properties of the model, most notably the flux-induced topological Lifshitz transitions are shifted towards the values of the flux per a diatomic plaquette (f) close to the flux quantum ($f \sim 1/2$). Geometrical frustration of the lattice breaks the $k \rightarrow \pi - k$ particle-hole spectral symmetry present in non-frustrated ladders, and leads to splitting of the degeneracies at metal-insulator transitions. A remarkable feature of a translationally invariant triangular ladder is the appearance of isolated Dirac node at the Brillouin zone boundary, rendering the ground state at $f = 1/2$ semi-metallic. We calculate the flux dependence of the orbital current and identify Lifshitz critical points by the singularities in this dependence at a constant chemical potential μ and constant particle density ρ . The absence of the particle-hole symmetry in the triangular ladder leads to the asymmetry between particle ($\rho > 1$) and hole ($\rho < 1$) doping and to qualitatively different results for the phase diagram, Lifshitz points and the flux dependence of the orbital current in the settings $\rho = \text{const}$ and $\mu = \text{const}$.

I. INTRODUCTION

The effects caused by an external magnetic field that quantizes the spectrum of charged carriers in crystalline lattices has long been one of fundamental problems in condensed matter physics [1–8]. The interplay of the applied magnetic field, dynamical correlations between the particles and superimposed geometrical lattice frustration has become the subject of intense research in recent years. Main objects of these studies are Fermi and Bose gases on ladders, which are minimal quasi-one-dimensional structures that can accommodate finite magnetic fluxes through elementary plaquettes. The kinetic frustration caused by the magnetic field, as well as the geometrical frustration present in structures like triangular and Creutz ladders, dramatically change the properties of a system when the flux per particle is close to one (more generally, rational fraction of) flux quantum [9, 10]. In naturally existing quasi-one-dimensional electron systems so strong fields could hardly be achieved. More-

over, in such objects the possibility to focus on purely orbital effects of the magnetic flux would be obscured by Zeeman splitting of the electron spin states. Fortunately, ultracold atoms represent an excellent opportunity to circumvent these limitations. It has been demonstrated [11] that, in systems of neutral atoms on optical lattices, Raman-assisted tunneling in two-dimensional optical lattices generates synthetic gauge fields and thus makes high effective fluxes feasible. Moreover, lattice connectivity in optical multi-leg flux ladders can be ensured by an extra synthetic dimensions which can be engineered taking advantage of the internal atomic degrees of freedom [12, 13].

The properties of bosonic and fermionic flux ladders have been the subject of many theoretical and experimental studies [14–24]. Ground state phases and their topological properties, chiral boundary currents and topological Lifshitz transitions taking place in ladders on varying the flux have been investigated. Lifshitz transitions connect phases with different numbers of Fermi points in the band spectrum and reveal them-

selves through the singularities in the flux dependence of the persistent orbital current and its derivative – the charge stiffness. The existence of cusps in this dependence for a half-filled standard (square) ladder was indicated in Refs.[18, 19] and more recently in Refs.[20, 24]. Away from half-filling, the behavior of the orbital current as a function of the flux essentially depends on which quantity, the particle density $\rho = N_f/N$ (canonical ensemble) or the chemical potential μ (grand canonical ensemble), is chosen to be a fixed parameter [24]. In standard experiments with ultracold atoms the density is fixed. However, interesting proposals to control the chemical potential in such systems have recently been reported. These include splitting of two-dimensional ultracold atom systems into a physical sample of a homogeneous density and a dilute reservoir using advances in quantum gas microscopy [25], realization of two-terminal configurations based on holographic techniques for the study of Landauer transport [26], and the effective control of chemical potentials using Rabi coupling between different hyperfine levels of the atomic species [27].

In this paper we consider a triangular fermionic ladder which consists of two chains coupled by an asymmetric single-particle hopping across zigzag-like interchain links. The properties of the system are formed due to the combined effect of geometrical frustration of the lattice and magnetic flux. Here we will resort to a model of noninteracting fermions postponing the study of correlation effects until a separate forthcoming publication [28]. To extract purely orbital effects of the flux we assume that the particles are spinless. In a standard ladder, even in the presence of the flux the two-band spectrum maintains a $k \rightarrow \pi - k$ perfect nesting property. On the contrary, in a triangular ladder geometrical frustration entails a dispersive character of interchain hopping, and the latter in turn leads to the breakdown of the particle-hole (ph) symmetry. For a weak interchain coupling, the difference between the two ladders is most pronounced when the flux per particle is close to flux quantum. The spectrum of the triangular ladder acquires a new feature: the appearance of two groups of Dirac-like low-energy excitations with different masses. In particular, in a symmetric (translationally invariant) triangular ladder one of the mass gaps vanishes, and the spectrum exhibits an

isolated Dirac node at the Brillouin zone boundary. Close to half-filling this leads to a qualitative difference between the ground states of the standard and symmetric triangular ladders: the former is insulating while the latter represents a semi-metal susceptible to quantum dynamical fluctuations. The absence of ph -symmetry in the triangular ladder to the asymmetry between particle and hole doping and to qualitatively different results for the phase diagram, Lifshitz points and the flux dependence of the orbital current in the settings with $\rho = \text{const}$ and $\mu = \text{const}$.

The paper is organized as follows. In Sec.II we introduce the triangular flux-ladder (TFL) model in the absence of interactions and discuss its spectral properties assuming that interchain single-particle hopping is weak. We pay special attention to those features of the model which are caused by geometrical frustration of the lattice. For weakly coupled chains, the representation of the low-energy part of the spectrum in terms of two groups of massive Dirac fermion proves efficient for the study of topological Lifshitz transitions for the flux is close to a flux quantum per plaquette. In Sec.III we provide gauge invariant definitions of the total and relative currents, give general expressions for their ground-state expectation values and fully characterize their symmetry properties. In Sec.IV we calculate the orbital current at a fixed chemical potential ($\mu = 0$). We show that the difference between the Dirac masses, caused by the lattice geometrical frustration, leads to a sequence of two commensurate-incommensurate transitions showing up as universal square-root singularities in the flux dependence of the current. In Sec.V we describe Lifshitz transitions between various ground-state phases at a constant particle density ρ assuming that the value of the flux per plaquette is close to one flux quantum. We separately consider the cases of hole ($\rho < 1$) and particle ($\rho > 1$) doping, identify Lifshitz transitions by the cusps in the flux dependence of the orbital current and emphasize a qualitative difference between the phase diagrams in the two cases. The summary of the obtained results including suggestions of their further generalizations is compiled in Sec.VI.

II. TRIANGULAR LADDER

A frustrated ladder with a zigzag geometry of interchain links is shown in Fig.1. We use the longitudinal gauge in which the flux through the Peierls substitution affects only hopping along the chains. The case $t_1 = t_2$ corresponds to a translationally invariant ladder. When one of the two amplitudes, t_1 or t_2 , vanishes, the triangular ladder becomes topologically equivalent to a standard (rectangular) ladder. In the absence of interactions the Hamiltonian of the TFL reads

$$H = -t_0 \sum_n \sum_{\sigma=\pm} (c_{n\sigma}^\dagger c_{n+1,\sigma} e^{-i\sigma\pi f} + h.c.) - \sum_n (t_1 c_{n+}^\dagger c_{n-} + t_2 c_{n+}^\dagger c_{n-1,-} + h.c.) \quad (1)$$

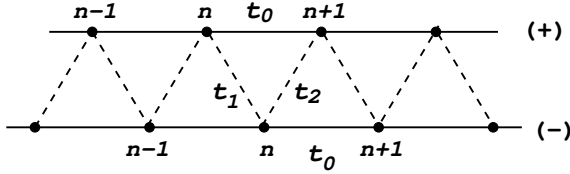


FIG. 1: Triangular ladder. The integer n labels the diatomic unit cells. t_0 , t_1 and t_2 stand for the amplitudes of single-particle nearest-neighbor hopping along the chains and between them.

Here $c_{n\sigma}$ and $c_{n\sigma}^\dagger$ are second-quantized operators for a spinless fermion on the lattice site (n, σ) , the index $\sigma = \pm$ labels the chains, and $f = \Phi_{\square}/\phi_0$ is the flux per the diatomic plaquette in units of the flux quantum $\phi_0 = hc/e$. In momentum representation

$$H = \sum_k \psi_k^\dagger \hat{\mathcal{H}}(k) \psi_k, \quad \psi_k = \begin{pmatrix} c_{k+} \\ c_{k-} \end{pmatrix} \quad (2)$$

Here

$$\hat{\mathcal{H}}(k) = \epsilon(k) - \mathbf{h}(k) \cdot \hat{\boldsymbol{\sigma}} \quad (3)$$

is a 2×2 matrix form of the first quantized Hamiltonian whose scalar and vector parts are given by

$$\epsilon(k) = -2t_0 \cos(\pi f) \cos k, \quad \mathbf{h}(k) = \{t_1 + t_2 \cos k, t_2 \sin k, 2t_0 \sin(\pi f) \sin k\} \quad (4)$$

The quasi-momentum k , measured in units of inverse lattice spacing $1/a_0$, varies within the Brillouin zone,

$|k| < \pi$, and the Pauli matrices $\hat{\sigma}_a$ ($a = 1, 2, 3$) act in the two-dimensional space of the Nambu spinor ψ_k . The spectrum of H_0 consists of two bands labeled by the index $s = \pm$:

$$E_s(k) = -2t_0 \cos(\pi f) \cos k + sE_k, \quad E_k = |\mathbf{h}(k)| \quad (5)$$

Throughout this paper we assume that the interchain tunneling amplitudes are positive and small, $0 < t_{1,2} \ll t_0$. Moreover, we restrict consideration to the case when the particle density $\rho = N^{-1} \sum_{n\sigma} \langle c_{n\sigma}^\dagger c_{n\sigma} \rangle$ is equal or close to 1. Accordingly the chemical potential is small, $|\mu| \ll 2t_0$. Without loss of generality, everywhere below we will assume that $t_1, t_2 > 0$.

In the standard ladder ($t_1 t_2 = 0$), for any f the band spectrum (5) has the property [18, 19]:

$$E_s(k + \pi) = -E_{-s}(k) \quad (6)$$

This symmetry is generated by a staggered particle-hole (ph) transformation of the fermionic operators, $c_{k\sigma} \rightarrow c_{k+\pi, -\sigma}^\dagger$. As a result, if the particle density is fixed at $\rho = 1$, Eq.(6) necessarily leads to a half-filled band spectrum and vanishing chemical potential, and vice versa. The spectral properties of the standard ladder at $\rho < 1$ and $\rho > 1$ (equivalently, for the values of the chemical potential $\pm\mu$) are equivalent. In the metallic phase of a half-filled ladder, the Fermi momenta at any f form pairs $\pm(k_F, \pi - k_F)$.

As follows from (5), this is not the case for a TFL ($t_1 t_2 \neq 0$), where geometrical lattice frustration makes the band splitting momentum dependent. In Eq.(3) the "magnetic field" $|\mathbf{h}(k)|$ is not invariant under the transformation $k \rightarrow \pi \pm k$, and the perfect nesting property (6) is absent. As a consequence, for a general set of the parameters of the TFL, if the particle density is fixed at $\rho = 1$, the corresponding value of the chemical potential $\mu \neq 0$; inversely, if $\mu = 0$, then $\rho \neq 1$. The properties of the TFL at $\rho < 1$ and $\rho > 1$ are different. For a special value of the flux, $f = 1/2$, the Hamiltonian takes the Bloch form $\hat{\mathcal{H}}_k = -\mathbf{h}(k) \cdot \boldsymbol{\sigma}$ which implies the $(E, -E)$ symmetry of the band spectrum. Nevertheless the $k \rightarrow \pi - k$ symmetry is absent at $f = 1/2$ as well.

At weak interchain tunneling the loss of the ph -symmetry and all qualitative changes in structure of the spectrum are most pronounced in the limit $|t_1 - t_2| \ll t_1 + t_2$ and for the values of the flux f close to

1/2. Using the parametrization

$$f = \frac{1}{2} - \frac{\kappa}{2\pi t_0}, \quad |\kappa| \ll 2t_0 \quad (7)$$

and replacing (5) by the approximate expression

$$E_{\pm}(k) \simeq -\kappa \cos k \pm \sqrt{4t_0^2 \sin^2 k + t_1^2 + t_2^2 + 2t_1 t_2 \cos k + O(\kappa^2)} \quad (8)$$

we find that the low-energy states of the spectrum, $|E_{\pm}(k)| \ll 2t_0$, are located close to the points $k = 0$ and $k = \pi$, where excitations are described in terms of two groups of "massive Dirac fermions"

$$|k| \ll 1 : E_{\pm}(k) \simeq -\kappa \pm \sqrt{k^2 v_F^2 + M^2} \quad (9)$$

$$|k - \pi| \ll 1 : E_{\pm}(k) \simeq \kappa \pm \sqrt{(k - \pi)^2 v_F^2 + m^2} \quad (10)$$

Here $M = t_1 + t_2$, $m = t_1 - t_2$ and $v_F = 2t_0 a_0$ is the Fermi velocity (here we drop small corrections to v_F of the order $O(t_{1,2}^2)$). Both masses are small compared to $2t_0$.

In fact, the same type of the spectrum characterizes a family of frustrated two-leg ladders encapsulated in the asymmetric Creutz model, shown in Fig.2. Apart from the standard on-rung interchain tunneling (t_{\perp}), this model includes hopping across the diagonals of elementary plaquettes, parametrized by two independent amplitudes \tilde{t}_1 and \tilde{t}_2 . The case $\tilde{t}_1 = \tilde{t}_2 = 0$, $t_{\perp} \neq 0$ corresponds to a standard (non-frustrated) ladder. At $\tilde{t}_1 = \tilde{t}_2 \neq 0$ Fig.2 represents a symmetric Creutz ladder [29]. At $\tilde{t}_2 = 0$ one of the diagonals of the plaquette is disabled and the lattice becomes topologically equivalent to a triangular ladder with alternating interchain tunneling amplitudes t_{\perp} and \tilde{t}_1 ; in the notations of the model (1) the latter coincide with t_1 and t_2 , respectively.

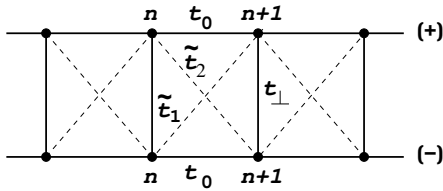


FIG. 2: Asymmetric Creutz ladder.

In the presence of the flux f the Hamiltonian $\hat{\mathcal{H}}(k)$ of the asymmetric Creutz ladder has the form (3) with

$$\mathbf{h}(k) = \{t_{\perp} + (\tilde{t}_1 + \tilde{t}_2) \cos k, (\tilde{t}_1 - \tilde{t}_2) \sin k, 2t_0 \sin(\pi f) \sin k\}$$

The low-energy part of its spectrum is given by formulas (9), (10) with the Dirac masses $M = t_{\perp} + \tilde{t}_1 + \tilde{t}_2$ and $m = t_{\perp} - \tilde{t}_1 - \tilde{t}_2$. The asymmetry parameter $\tilde{t}_1 - \tilde{t}_2$ is the measure of geometrical frustration of the model of Fig.2. The TFL is the maximally frustrated member of this family. In the rest of this paper we will only deal with the TFL.

Turning back to the model (3)–(4), we choose for certainty $t_1 \geq t_2 \geq 0$ and introduce a frustration parameter

$$\delta = \frac{t_2}{t_1} = \frac{M - m}{M + m}, \quad 0 \leq \delta \leq 1 \quad (11)$$

In the standard ladder ($\delta = 0$), the $k \rightarrow k + \pi$ symmetry keeps the masses equal; Fig.3a. Geometrical frustration ($\delta \neq 0$) makes the Dirac masses different: see Fig.3b. The difference is most striking in the translationally invariant case ($m \rightarrow 0$), when the degree of frustration reaches its maximum, $\delta \rightarrow 1$; Fig.3c. While at $f = 1/2$ ($\kappa = 0$), the ground state of a half-filled standard ladder is insulating, under the same conditions the presence of a Dirac node at $k = \pi$ renders the spectrum of the symmetric TFL gapless [43] (Fig.3c).

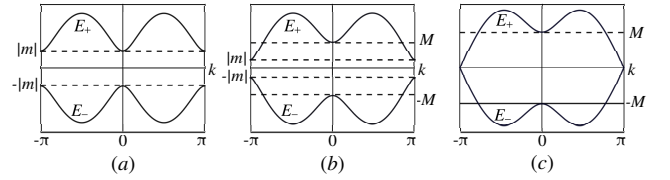


FIG. 3: Band spectrum at $f = 1/2$ a) in the standard ladder, b) in the triangular ladder at $m \neq 0$, c) in the triangular ladder at $m = 0$.

The appearance of the parameter κ in the expressions (9), (10) makes the spectrum deformable: when κ is varied, the parts of the dispersion curves at $k \sim 0$ and $k \sim \pi$ "move" along the energy axis in opposite directions. This fact explains the existence of flux induced topological Lifshitz transitions [33] between ground state phases with different numbers of Fermi points. Moreover, it also indicates that, as long as $|\mu|, M, |m| \ll 2t_0$, all these transitions take place in the vicinity of the point $f = 1/2$, i.e. at small κ . The difference between the mass gaps M and $|m|$ affects the ground state phase diagram and the sequence of Lifshitz transitions in a TFL even at $\mu = 0$. The

transitions show up in the experimentally observable singularities in the flux dependence of the orbital current and the anomalies of the charge stiffness of the system. A discussion on this issue in the context of square flux ladders, together with relevant references to ongoing experimental work, can be found in the recent publication [24].

To complete this section, let us briefly comment on topological properties of the insulating phases of the noninteracting TFL. For instance, at $f = 1/2$ such phases are realized at $m \neq 0$ under the condition that $-|m| < \mu < |m|$. With $M > 0$ there are two insulating phases corresponding to opposite signs of the mass m (of course, the thermodynamical properties depend only on $|m|$). The topological properties of a gapped ground state can be inferred from the 2×2 matrix structure of the Bloch Hamiltonian $\hat{\mathcal{H}}(k) = -\mathbf{h}(k) \cdot \hat{\sigma}$ in Eq.(3). In spite of the different structure of the Nambu spinors, the first quantized Hamiltonian $\hat{\mathcal{H}}(k)$ of the TFL and that of the 1D spinless p-wave superconductor (Kitaev's model) [30, 31] have the same matrix form and same symmetry properties of the "magnetic" field $\mathbf{h}(k)$ under transformation $k \rightarrow -k$. According to conventional definitions (see e.g. Ref. 32), a matrix Hamiltonian $\mathcal{H}(k)$ possesses time reversal (\mathcal{T}), charge-conjugation (\mathcal{C}) and chiral (\mathcal{S}) symmetry if the following conditions

$$\begin{aligned} U_{\mathcal{T}} \mathcal{H}^*(k) U_{\mathcal{T}}^{-1} &= \mathcal{H}(-k) \\ U_{\mathcal{C}} \mathcal{H}^*(k) U_{\mathcal{C}}^{-1} &= -\mathcal{H}(-k) \\ U_{\mathcal{S}} \mathcal{H}(k) U_{\mathcal{S}}^{-1} &= -\mathcal{H}(k) \end{aligned}$$

are satisfied (here the U s are unitary matrices). Apparently, charge conjugation symmetry is present (with $U_{\mathcal{C}} = \sigma_3$), whereas time reversal and chiral symmetries are explicitly broken. These facts place the TFL into the symmetry class D [32]. In this class, maps of the Brillouin zone to the sphere traversed by a unit vector $\mathbf{h}(k)/|\mathbf{h}(k)|$ form a \mathbb{Z}_2 group. Following the same arguments as those in [31], one finds out that homotopically nontrivial maps take place at $m < 0$ (more generally at $Mm < 0$). Thus the insulating ground state of the TFL at $m < 0$ is topologically nontrivial, characterized by a nonzero Zak phase $\phi_{\text{Zak}} = \pi$, whereas the phase at $m > 0$ is nontopological ($\phi_{\text{Zak}} = 0$). It is clear that the insulating phase of

a standard ladder with $M = m$ is topologically trivial.

III. ORBITAL CURRENT

The gauge invariant current through a directed link $\langle n, n+1 \rangle$ of the chain σ is defined as

$$J_{n,n+1}^{\sigma} = -it_0 c_{n\sigma}^{\dagger} c_{n+1,\sigma} e^{-i\pi\sigma f} + h.c., \quad (\sigma = \pm)$$

The second quantized total and relative current operators are given by

$$J_{\text{tot}} = N^{-1} \sum_{n\sigma} J_{n,n+1}^{\sigma} = N^{-1} \sum_k \psi_k^{\dagger} \hat{J}_{\text{tot}}(k) \psi_k \quad (12)$$

$$J_{\text{rel}} = N^{-1} \sum_{n\sigma} \sigma J_{n,n+1}^{\sigma} = N^{-1} \sum_k \psi_k^{\dagger} \hat{J}_{\text{rel}}(k) \psi_k \quad (13)$$

where

$$\hat{J}_{\text{tot}}(k) = 2t_0 [\cos(\pi f) \sin k - \hat{\sigma}_3 \sin(\pi f) \cos k] \quad (14)$$

$$\hat{J}_{\text{rel}}(k) = 2t_0 [\hat{\sigma}_3 \cos(\pi f) \sin k - \sin(\pi f) \cos k] \quad (15)$$

are first quantized 2×2 matrix versions of the currents in the chain basis.

The Hamiltonian (3) is invariant under parity transformation P ($k \rightarrow -k$) combined with the interchange of the two chains of the ladder P_{12} ($\sigma \rightarrow -\sigma$):

$$\mathcal{P} = PP_{12}, \quad \mathcal{P} \hat{\mathcal{H}}(k) \mathcal{P}^{-1} = \hat{\sigma}_1 \hat{\mathcal{H}}(-k) \hat{\sigma}_1 = \hat{\mathcal{H}}(k) \quad (16)$$

Under \mathcal{P} the total current $\hat{J}_{\text{tot}}(k)$ changes its sign. Therefore, as long as this symmetry remain unbroken, which is an obvious case for the noninteracting model, the expectation value of the total current vanishes. This conclusion can be changed in strongly correlated phases of interacting fermions in which \mathcal{P} -symmetry may be spontaneously broken [28]. On the other hand, the operator $\hat{J}_{\text{rel}}(k)$ remains invariant under \mathcal{P} and, hence, except for special values of f , its expectation value is nonzero. Thus, at $f \neq 0$ the ground state of the TFL is characterized by a nonzero orbital current $\langle \hat{J}_{\text{rel}} \rangle$ flowing in opposite directions on the upper and lower chains (Fig.4).

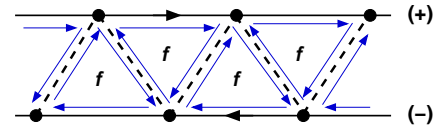


FIG. 4: Right and left fermions propagate along the upper ($\sigma = +$) and lower ($\sigma = -$) chains, respectively. Net local currents along the zigzag links vanish.

The ground state expectation value of the orbital current is given by

$$\begin{aligned} \mathcal{J}(f) &\equiv \langle J_{\text{rel}} \rangle \\ &= \frac{2t_0}{N} \sum_{k\sigma} \langle c_{k\sigma}^\dagger c_{k\sigma} \rangle [\sigma \sin k \cos(\pi f) - \cos k \sin(\pi f)] \end{aligned} \quad (17)$$

The occupation numbers $\langle c_{k\sigma}^\dagger c_{k\sigma} \rangle$ can be easily computed using the Matsubara Green's function in the 2×2 matrix representation, $\hat{G}(k, \varepsilon) = (\text{i}\varepsilon + \mu - \hat{\mathcal{H}}_k)^{-1}$, with $\hat{\mathcal{H}}_k$ given by (3). The result is

$$\begin{aligned} \mathcal{J}(f) &= -\frac{2t_0}{\pi} \int_0^\pi dk \mathcal{F}(k; f), \\ \mathcal{F}(k; f) &= \left\{ \frac{t_0 \sin(2\pi f) \sin^2 k}{E_k} \times [n_+(k) - n_-(k)] \right. \\ &\quad \left. + \cos k \sin(\pi f) [n_+(k) + n_-(k)] \right\} \end{aligned} \quad (18)$$

where E_k is given by (5) and $n_\pm(k) = \theta[\mu - E_\pm(k)]$ are the ground state Fermi distribution functions for the upper and lower bands, $\theta(x)$ being the Heaviside step function. As follows from (18), the orbital current is contributed by *all* occupied state of the two-band spectrum and, as has been mentioned earlier [18, 19], does not represent an infrared phenomenon.

For arbitrary values of the chemical potential μ the current vanishes at integer values of the flux, $f = 0, \pm 1, \pm 2, \dots$, and has the periodicity property $\mathcal{J}(f+2) = \mathcal{J}(f)$. At the special value $f = 1/2$

$$\mathcal{J}(1/2) = -\frac{2t_0}{\pi} \int_0^\pi dk \cos k [n_+(k) + n_-(k)] \quad (19)$$

When $m \neq 0$ and μ lies within the spectral gap (see Fig.3b), $-|m| \leq \mu \leq |m|$, the ground state is insulating with an empty upper band $E^+(k)$ and fully filled lower band $E^-(k)$. In this case for all k $n_+(k) = 0$, $n_-(k) = 1$, and the integral in (19) vanishes: $\mathcal{J}(1/2)|_{\text{insul}} = 0$. This result is valid for all $f = l + 1/2$ as long as the ground state is insulating. If $\mu > |m|$ or $\mu < -|m|$, a "Fermi surface" appears and the ground state becomes metallic with a finite k_F , in which case $\mathcal{J}(1/2) \sim \sin k_F \neq 0$.

Shifting the flux by one flux quantum, $f \rightarrow f+1$, or inverting it with respect to the point $1/2$, $f \rightarrow 1-f$, generates a non-staggered *ph*-transformation of the band spectrum, $E_s(k, 1 \pm f) = -E_{-s}(k, f)$. Accordingly $n_\pm(k; 1-f, \mu) = 1 - n_\mp(k; f, -\mu)$. Then

from the definition (18) it follows that

$$\mathcal{J}(f+1; \mu) = \mathcal{J}(f; -\mu) \quad (20)$$

$$\mathcal{J}(1-f; \mu) = -\mathcal{J}(f; -\mu) \quad (21)$$

When the current is defined at a fixed density ρ , the above transformation should be replaced by

$$\mathcal{J}(f+1; \rho) = \mathcal{J}(f; 2-\rho) \quad (22)$$

$$\mathcal{J}(1-f; \rho) = -\mathcal{J}(f; 2-\rho) \quad (23)$$

Thus, in the TFL, the orbital current is symmetric (antisymmetric) under transformations $f \rightarrow f+1$ ($f \rightarrow 1-f$) combined with particle-hole transformations $\mu \rightarrow -\mu$ or $\rho \rightarrow 2-\rho$. For comparison, for a standard ladder, the spectral property (6) makes the current symmetric under the change $\mu \rightarrow -\mu$, and $\mathcal{J}(f)$ is a periodic function of the flux with the period $\Delta f = 1$.

IV. COMMENSURATE-INCOMMENSURATE TRANSITIONS AT CONSTANT CHEMICAL POTENTIAL

At $f \ll 1$ the current is proportional to the flux and the difference between the standard and triangular ladders is not significant. Below we concentrate on the region $|f - 1/2| \ll 1$. Here we will assume that the TFL is in contact with a reservoir which supports a fixed value of the chemical potential $\mu = 0$. This value of μ is chosen only for the sake of simplicity of the discussion. We will show that geometrical frustration of the TFL splits the Lifshitz (metal-insulator) transition of the square ladder into two consecutive transitions taking place at $\kappa = |m|$ and $\kappa = M$. In the vicinity of these transitions the current is a non-analytic function of the flux.

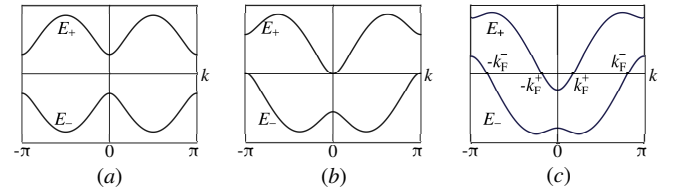


FIG. 5: Commensurate-incommensurate transition in a standard ladder. a) Insulating phase at $\kappa < |m|$; b) critical point $\kappa = |m|$; c) metallic phase at $\kappa > |m|$.

Using (7) and the expression (8) valid at small κ , we represent the current as

$$\mathcal{J}(\kappa) = -\frac{1}{\pi} \sum_{s=\pm} \int_0^\pi dk \Phi_s(k) n_s(k), \quad (24)$$

$$\Phi_s(k) = W \cos k + s \frac{\kappa \sin^2 k}{\mathcal{E}_k},$$

$$\mathcal{E}(k) = \sqrt{\sin^2 k + \tau_1^2 + \tau_2^2 + 2\tau_1\tau_2 \cos k}$$

where $W = 2t_0$ and $\tau_{1,2} = t_{1,2}/W \ll 1$.

We start with the insulating phase at $m \neq 0$, Fig.3b, realized at $\kappa < |m|$. For this phase $n_+(k) = 0$, $n_-(k) = 1$ for all k , and the orbital current is a linear function of κ . With the logarithmic accuracy

$$\begin{aligned} \mathcal{J}_0(\kappa) &= \frac{C_0}{\pi} \kappa, \\ C_0 &= \int_0^\pi dk \frac{\sin^2 k}{\mathcal{E}_k} \\ &= 2 - \frac{1}{2W^2} \left(M^2 \ln \frac{W}{M} + m^2 \ln \frac{W}{|m|} \right) \end{aligned} \quad (25)$$

For the insulating phase of the standard ladder the result is not much different: one only has to set in (25) $M = m$. The difference emerges when the transitions to metallic phases are compared. For a half-filled standard ladder, the ph -symmetry (6) implies that if for some κ $E_+(0) = 0$, then necessarily $E_-(\pi) = 0$. Fig.5b shows the spectrum at the doubly degenerate critical point $\kappa = m = t_1$. As follows from Fig.5c, at $\kappa > m$ the ground state becomes metallic with *four* Fermi points, $\pm k_0$, and $\pm(\pi - k_0)$. In this phase, close to the critical point $k_0 = \sqrt{\kappa^2 - m^2}/v_F$. One then finds that

$$\mathcal{J}(\kappa) = \mathcal{J}_0(\kappa) + \mathcal{J}_{\text{sing}}(\kappa) \quad (26)$$

where the singular part of the current displays a square-root dependence on κ , typical for a quantum commensurate-incommensurate (C-IC) transition [34, 35]:

$$\begin{aligned} \mathcal{J}_{\text{sing}}(\kappa) &= -\frac{W}{\pi} \left(\int_0^{k_0} + \int_0^{\pi-k_0} \right) dk \cos k \\ &= -\frac{2}{\pi} \sqrt{\kappa^2 - m^2} + O[(\kappa^2 - m^2)^{3/2}] \end{aligned} \quad (27)$$

As already mentioned, in the TFL, an arbitrarily weak frustration ($\delta \ll 1$) removes the degeneracy of the two mass gaps, which leads to two Lifshitz transitions. Increasing κ in the insulating phase, Fig.3b,

one first observes a transition at $\kappa = |m|$, where $E_-(\pi; |m|) = 0$ with $E_+(0; |m|) > 0$. This is a transition to a metallic phase with *two* Fermi points, shown in Fig.6a. This phase is realized in the region $|m| < \kappa < M$. Close to the critical point $0 < \kappa - |m| \ll |m|$ one obtains $\mathcal{J}_{\text{sing}}(\kappa) \simeq \pi^{-1} \sqrt{\kappa^2 - m^2}$. Further increasing κ leads to the second Lifshitz transition to a metallic phase with *four* Fermi points, Fig. 6b. This transition occurs at $\kappa = M$ where $E_+(0; M) = 0$. One then finds that $\mathcal{J}_{\text{sing}}(\kappa) \simeq -\pi^{-1} \sqrt{\kappa^2 - M^2}$ at $0 < \kappa - M \ll M$. At larger values of κ , namely at $M \ll \kappa \ll W \ln^{-1/2}(W/M)$, the current is easily shown to be inversely proportional to κ : $\mathcal{J}(\kappa) \simeq (M^2 + m^2)/2\pi\kappa$.

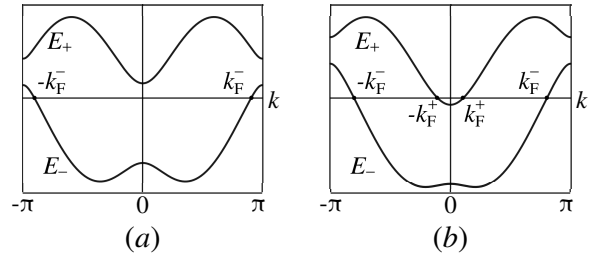


FIG. 6: Commensurate-incommensurate transition in a TFL. a) 2FP metallic phase at $|m| < \kappa < M$; b) 4FP metallic phase at $\kappa > M$.

At $m \rightarrow 0$ the insulating phase of the TFL disappears, implying that the transition at $\kappa = |m|$ disappears as well. The phase at $0 < \kappa < M$ is metallic with *two* Fermi points. The current in this region is a linear function of κ but with a different slope as compared to Eq.(25):

$$\mathcal{J}(\kappa) = \frac{\kappa}{\pi} \left(1 - \frac{M^2}{2W^2} \ln \frac{W}{M} \right) \quad (28)$$

At $\kappa = M$ the ladder crosses over to the metallic state with four Fermi points. The flux dependence of the orbital current at $m \neq 0$ and small κ is shown in Figs.7. The quantity diverging at the C-IC transitions is the relative charge stiffness defined as a response function [36, 37]

$$D = \frac{1}{2\phi_0} \frac{\partial \mathcal{J}}{\partial f} = -\frac{\pi t_0}{\phi_0} \frac{\partial \mathcal{J}}{\partial \kappa} \quad (29)$$

In the context of usual C-IC transitions taking place in the charge or spin excitations of various one-dimensional Fermi systems [38], the quantity D is

similar to the compressibility or spin susceptibility. We see that, when the frustration ratio δ , Eq.(11), is nonzero, the single peak of D at the metal-insulator transition of the standard ladder splits into two peaks that move apart as δ is increased (Figs.7). In the vicinity of these transitions $D(\kappa)$ displays universal square-root singularities [34, 35]:

$$D(\kappa) \simeq \frac{t_0}{\phi_0} \frac{\kappa_c}{\sqrt{\kappa^2 - \kappa_c^2}} \theta(\kappa^2 - \kappa_c^2) \quad (30)$$

with $\kappa_c = |m|$ or M .

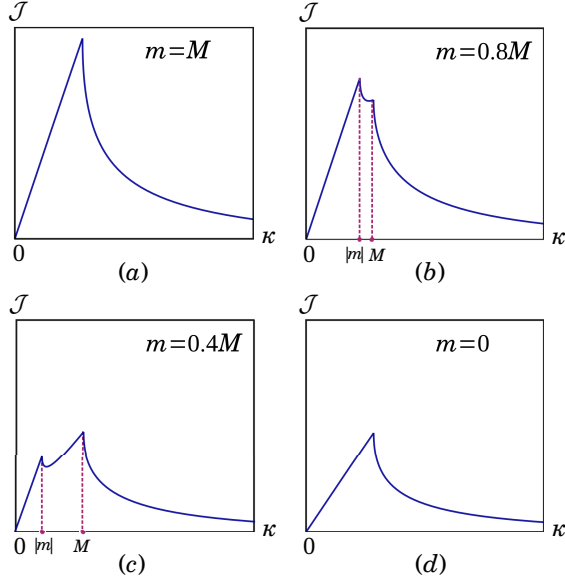


FIG. 7: Orbital current at a fixed chemical potential $\mu = 0$ and small κ for different values of $|m|$, with $M = 0.4t_0$. (a) A single Lifshitz transition in a standard ladder, $|m| = M$; (b) and (c) – a sequence of two transitions at $|m| < M$; (d) a single transition at $\kappa = M$ when $m \rightarrow 0$.

Ground state phases and the transitions between them at a small nonzero μ can be categorized along the same lines. At a constant $\mu \neq 0$ all Lifshitz transitions accessed by varying the flux belong to the C-IC universality class, with a typical behavior of the charge stiffness given by (30). The reason for that is simple. A generic C-IC transition is a transition from an insulator with a parabolic two-band spectrum to a metal, taking place when varying the chemical potential leads to the appearance of extra particles(holes) in the conduction (valence) band. In the TFL with a constant μ the deformation of the two-band spectrum caused by a small κ can be recast as the appearance of variable effective chemical potentials in the Dirac-like

parts of the spectrum in the regions $k \sim 0$ and π . Repopulation of these low-energy states in each of these region occurs independently and at different values of κ . Therefore, each of these transitions is of the C-IC type.

V. PHASE DIAGRAM AND ORBITAL CURRENT AT CONSTANT DENSITY

In this section we discuss the effect of the flux on the spectrum, orbital current and phase diagram of the noninteracting TFL at a constant density, fixed at a value close to 1: $\rho = 1 + n$, $|n| \ll 1$. Such setup is typical for ultracold atoms on optical lattices. As before, we assume that $|f - 1/2| \ll 1$. Except for the special case $\rho = 1$, Lifshitz transitions at $\rho = \text{const}$ are different from those that occur at $\mu = \text{const}$. Moreover, as we show below, contrary to the standard ladder, in the TFL the absence of ph -symmetry makes the pictures at hole doping ($n < 0$) and particle doping ($n > 0$) qualitatively different.

At $\kappa > (M + |m|)/2$ the two bands of the spectrum overlap. If the chemical potential is located between the energies $E_+(0)$ and $E_-(\pi)$, i.e. $M - \kappa < \mu < \kappa - |m|$, the ground state is metallic with four Fermi points $\pm k_F^+$, $\pm k_F^-$ in the spectrum. We will call this state the 4FP-phase. Imposing an additional restriction upon the density,

$$\pi|n| < \frac{\sqrt{M^2 - m^2}}{W} \quad (31)$$

we disregard the situation when $\mu < E_-(0)$ and all four Fermi points belong to the $E_-(k)$ band. Starting from the 4FP phase we will then trace its evolution as κ is decreased. At a constant density $\rho \neq 1$ the Fermi momenta k_F^\pm are subject to the constraint $k_F^+ + k_F^- = \pi(1 + n)$. Since $|\kappa| \ll W$ and $|n| \ll 1$, k_F^+ and k_F^- are close to the points $k = 0$ and π , respectively, where the spectrum has the Dirac form (9) and (10). Therefore we can set $k_F^+ = p_+$, $k_F^- = \pi - p_-$, where the momenta p_\pm are small, positive and satisfy

$$p_+ - p_- = \pi n \quad (32)$$

At given values of the Dirac masses the dependence of p_\pm and μ on the flux is described by the equations

$$\sqrt{p_+^2 v_F^2 + M^2} = \kappa + \mu, \quad \sqrt{p_-^2 v_F^2 + m^2} = \kappa - \mu \quad (33)$$

valid in the 4FP phase for any sign of n .

A. $\rho < 1$ ($n < 0$)

According to (32) at $n < 0$ one has $p_+ < p_-$. The momentum p_+ decreases with κ and vanishes at some critical value $\kappa = \kappa_c$ where the band $E_+(k)$ gets empty. This is a Lifshitz transition at which the number of Fermi points changes from four to two (Fig.8b); we label the new state as the 2FP phase. The critical values of κ and μ are given by $\kappa_c = (M + Q_m)/2$, $\mu_c = (M - Q_m)/2$, where $Q_m = \sqrt{(\pi n)^2 v_F^2 + m^2}$. As shown below, the dependence $p_+ = p_+(\kappa)$ at small $\kappa - \kappa_c$ determines the singularities in the flux dependence of the orbital current near the transition.

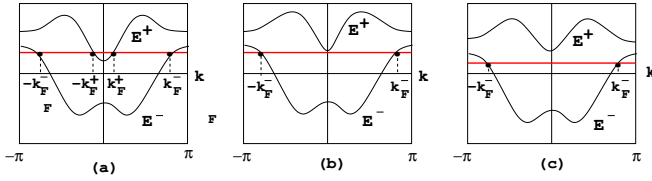


FIG. 8: Case $\rho < 1$. (a) 4FP metallic phase at $\kappa > \kappa_c$; (b) Lifshitz critical point at $\kappa = \kappa_c$; (c) 2FP metallic phase at $\kappa < \kappa_c$.

From (32 and (33) one derives the quadratic equation for p_+ valid in the 4FP-phase

$$Ap_+^2 + Bp_+ - C = 0, \quad \kappa > \kappa_c \quad (34)$$

where

$$A = 1 - \left(\frac{\pi|n|}{2\kappa} \right)^2, \quad B = \pi|n| \left(1 + \frac{\kappa_c \mu_c}{\kappa^2} \right), \quad C = \left(1 - \frac{\mu_c^2}{\kappa^2} \right) (\kappa^2 - \kappa_c^2) \quad (35)$$

Obviously $B > 0$. Since $\kappa > \kappa_c > \mu_c$, the coefficient C is positive as well. One also finds that

$$\frac{\pi|n|}{2\kappa} \leq \frac{\pi|n|}{M + \sqrt{(\pi n)^2 + m^2}} < 1$$

implying that $A > 0$. Focusing on the vicinity of the Lifshitz point we introduce the small parameter $\zeta = (\kappa - \kappa_c)/\kappa_c$, $0 < \zeta \ll 1$. The solution of Eq.(34) satisfying the boundary condition $p_+(0) = 0$ reads

$$p_+(\zeta) = \frac{M\pi|n|}{A(M + Q_m)} \left[\sqrt{1 + (\zeta/\zeta_0)} - 1 \right] \quad (36)$$

$$\zeta_0 = \frac{1}{2A} \frac{M(\pi n W)^2}{Q_m(M + Q_m)^2}$$

Eq.(36) is applicable at any $|n| \ll 1$. Assuming that $A \lesssim 1$ and $M \gg |m|$ one easily checks that for any $|n| \ll 1$ the parameter $\zeta_0 \ll 1$. Therefore there are two regions of small ζ . In the immediate vicinity of the transition point, $0 < \zeta \ll \zeta_0$, the dependence $p_+(\zeta)$ is linear

$$p_+ = \frac{1}{v_F} \frac{Q_m(M + Q_m)}{W^2(\pi|n|)} \zeta \quad (37)$$

At larger deviations from the criticality, $\zeta_0 \ll \zeta \ll 1$, this dependence crosses over to the square-root asymptotics

$$p_+ = \frac{1}{W} \sqrt{\frac{2MQ_m\zeta}{A}} \quad (38)$$

typical for a C-IC transition. In the limit $n \rightarrow 0$ ($\rho \rightarrow 1^-$) $\zeta_0 \rightarrow 0$ and the square-root dependence becomes exact: $p_+ = \sqrt{2M|m|\zeta}$.

At $\kappa < \kappa_c$ the spectrum describes the metallic 2FP phase, Fig.8c, in which k_F^- stays fixed at the value $\pi(1 - |n|)$ and does not depend on κ . As long as $\rho < 1$, the lower band $E_-(k)$ remains partially filled, so the 2FP phase is stable down to the point $\kappa = 0$ ($f = 1/2$). Thus, at hole doping the ground state of the TFL with $m \neq 0$ always remains metallic. On decreasing κ one finds a single Lifshitz transition separating the 4FP and 2FP phases.

In the 2FP phase the chemical potential is given by $\mu(\kappa) = \kappa - \sqrt{(\pi n)^2 W^2 + m^2}$. When $\rho \rightarrow 1^-$ ($n \rightarrow 0^-$), μ reaches the top of the band $E_-(k)$ (see Fig.9a)

$$\lim_{n \rightarrow 0} \mu(\kappa) = \kappa - |m| \quad (39)$$

and the latter becomes fully filled. At $m \neq 0$ the upper and lower bands are separated by a finite gap $2|m|$. However at $m = 0$ a Dirac node appears in the spectrum of the π -fermions at the energy $E_-(\pi) = \kappa$ and the chemical potential is located just at this energy: $\mu = \kappa$. This is a semimetallic phase with a single Dirac point and a fully filled "Dirac sea"; see Fig.9b.

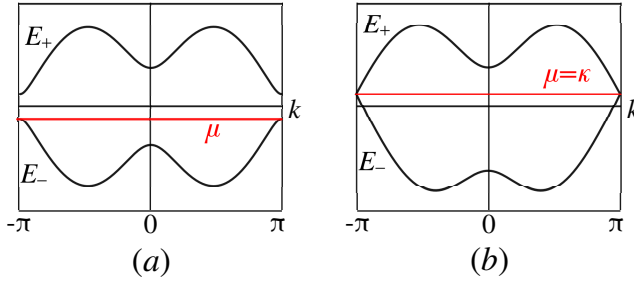


FIG. 9: $\rho = 1^-$. (a) $m \neq 0$; (b) $m = 0$.

Let us now estimate the orbital current at $\rho < 1$. According to the definition (24), in the 4FP phase the current is a sum of the contributions of the partially filled upper and lower bands:

$$\mathcal{J}_{4\text{FP}}(\kappa) = \mathcal{J}_+(\kappa) + \mathcal{J}_-(\kappa) = -\frac{1}{\pi} \sum_{s=\pm} \int_0^{k_F^s} dk \Phi_s(k) \quad (40)$$

where $k_F^- = \pi - p_+$ and $k_F^+ = p_+$ is given by (36). Since $k_F^+ \ll 1$, in the leading order

$$\mathcal{J}_+ = -\frac{W}{\pi} p_+ + O(p_+^3) \quad (41)$$

For \mathcal{J}_- we have

$$\begin{aligned} \mathcal{J}_- &= -\frac{1}{\pi} \left(\int_0^\pi - \int_{\pi-p_-}^\pi \right) dk \left(2t_0 \cos k - \frac{\kappa \sin^2 k}{\mathcal{E}_k} \right) \\ &\equiv \mathcal{J}_0 + \mathcal{J}_1 \end{aligned} \quad (42)$$

Here $\mathcal{J}_0 = C_0 \kappa / \pi$ given by (25) is the current in the band insulator phase, contributed by the fully filled band $E_-(k)$. For the integral \mathcal{J}_1 we obtain

$$\begin{aligned} \mathcal{J}_1 &= -\frac{W}{\pi} \sin \tilde{p}_+ - \frac{C_1 \kappa}{\pi} \\ C_1 &= \frac{m^2}{4W^2} (\sinh 2\alpha_0 - 2\alpha_0) \end{aligned} \quad (43)$$

where $\tilde{p}_+ = p_+ + \pi|n|$, $\sinh \alpha_0 = \tilde{p}_+ / |m|$. So, in the lowest order in the small parameters k_F^+ and $|n|$ the current in the 4FP phase can be written as

$$\mathcal{J}_{4\text{FP}}(\kappa) = -W|n| - \frac{2W}{\pi} k_F^+ + \frac{C_0 - C_1}{\pi} \kappa, \quad \kappa > \kappa_c \quad (44)$$

In the 2FP phase the upper band does not contribute to the current, so the latter is obtained from (44) by setting $p_+ = 0$. At $\kappa < \kappa_c$ the parameter C_1 depends only on the density $|n|$ and for any ratio $\pi|n|W/|m|$ is small compared to C_0 . Neglecting small corrections of the order of $M^2 \ln M$, we can write

$$\mathcal{J}_{2\text{FP}}(\kappa) = \frac{2}{\pi} (\kappa - \kappa_0), \quad \kappa_0 = t_0 \pi |n| \quad (\kappa < \kappa_c) \quad (45)$$

We see that, in the 2FP phase, the vacuum current is a linear function of κ . The point where it changes the sign is determined by the hole density $|n|$. The fact that $\mathcal{J}_{2\text{FP}}(0) \neq 0$ is not unexpected. It reflects the lack of the ph -symmetry of the model and the absence of the $\rho \rightarrow 2 - \rho$ invariance of the thermodynamic quantities (see the discussion in Sec.III).

Comparing (44) and (45) and taking into account (37) we observe that the current is continuous across the 2FP-to-4FP Lifshitz transition but exhibits a cusp at $\kappa = \kappa_c$. As a result, at the critical point the relative charge stiffness $D(\kappa)$, Eq.(29), which is proportional to the derivative $\partial \mathcal{J} / \partial \kappa$, undergoes a jump:

$$\left. \frac{\partial \mathcal{J}_{2\text{FP}}}{\partial \kappa} \right|_{\kappa_c} \equiv \lim_{\kappa \rightarrow \kappa_c - 0} \frac{\partial \mathcal{J}(\kappa)}{\partial \kappa} = \frac{2}{\pi} \quad (46)$$

$$\begin{aligned} \left. \frac{\partial \mathcal{J}_{4\text{FP}}}{\partial \kappa} \right|_{\kappa_c} &\equiv \lim_{\kappa \rightarrow \kappa_c + 0} \frac{\partial \mathcal{J}(\kappa)}{\partial \kappa} \\ &= \frac{2}{\pi} \left[1 - \sqrt{1 + \left(\frac{m}{\pi n W} \right)^2} \right], \quad n \neq 0 \end{aligned} \quad (47)$$

(In deriving formula (47) we neglected a small relative correction proportional to $\partial C_1 / \partial p_+$.) Thus, at a constant density but away from half-filling the square-root dependence of the current on the flux at the Lifshitz transition ($\kappa \rightarrow \kappa_c$), pertinent to C-IC transition in a grand-canonical ensemble, is replaced by a linear one. A similar situation has been described earlier [39] in the study of magnetization process of isolated 1D Fermi systems at a fixed particle number, and, more recently, in the context of standard ladders away from 1/2-filling [24].

B. $\rho > 1$ ($n > 0$)

Here again we start from the four-Fermi-point metallic state which we now label as the 4FP-1 phase. At $n > 0$ we have $p_+ > p_-$. On decreasing κ the first Lifshitz point $\kappa = \kappa_{c1}$ is reached, Fig.10a, at which $p_- = 0$ and the band $E^-(k)$ gets completely filled. The partial filling of the upper band $E^+(k)$ within the interval $|k| < k_F^+$ reflects the existence of a finite particle doping ($n = \rho - 1 > 0$). At the transition the number of Fermi points changes from four to two. We will label this phase as 2FP-1. We note that under the substitutions $p_+ \leftrightarrow p_-$, $M \leftrightarrow |m|$, $n \leftrightarrow -n$, $\mu \leftrightarrow -\mu$ the already discussed 4FP-2FP Lifshitz transition at

$\rho < 1$ exactly maps to the 4FP1-2FP1 transition at $\rho > 1$. Therefore the critical values of κ and μ are given by $\kappa_{c1} = (Q_M + |m|)/2$, $\mu_{c1} = (Q_M - |m|)/2$, with $Q_M = \sqrt{(\pi n)^2 W^2 + M^2}$, and, in the vicinity of the Lifshitz point, the flux dependence of the momentum $p_-(\kappa)$ is given by

$$p_- = \frac{|m|\pi n}{A(|m| + Q_M)} \left[\sqrt{1 + (\zeta/\zeta_1)} - 1 \right], \quad (48)$$

$$\zeta_1 = \frac{1}{2A} \frac{|m|(\pi n W)^2}{Q_M(|m| + Q_M)^2} \ll 1$$

where $\zeta_1 = (\kappa - \kappa_{c1})/\kappa_{c1}$ ($0 < \zeta \ll 1$). As in the $\rho < 1$ case, in (48) there are no restrictions on n except for $n \ll 1$. The smallness of ζ_1 implies the existence of the linear ($p_- \sim \zeta$) and square-root ($p_- \sim \sqrt{\zeta}$) asymptotics in the regions $\zeta \ll \zeta_1$ and $\zeta_1 \ll \zeta \ll 1$, respectively.

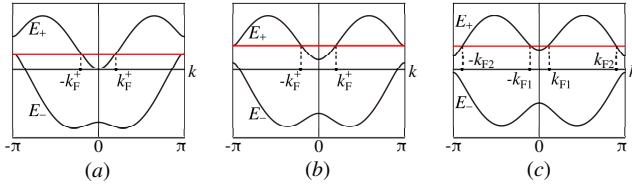


FIG. 10: Case $\rho > 1$. (a) Lifshitz transition at $\kappa = \kappa_{c1}$ between 4FP-1 to 2FP-1 phases; (b) Lifshitz transition at $\kappa = \kappa_{c2}$ between 2FP-1 to 4FP-2 phases; (c) 4FP-2 metallic phase at $\kappa < \kappa_{c2}$.

With k_F^+ fixed at the value $k_F^+ = \pi n > 0$, on decreasing κ with m kept finite one finds the second Lifshitz point $\kappa = \kappa_{c2} < \kappa_{c1}$ at which the chemical potential reaches the value $\mu = E^+(\pi)$ (see Fig.10b). The spectrum displays a re-entrant transition to another 4FP metallic phase which we denote by 4FP-2 (Fig.10c). One finds that $\kappa_{c2} = (Q_M - |m|)/2$, $\mu_{c2} = (Q_M + |m|)/2$. This critical point belongs to the region $(M + |m|)/2 < \kappa \ll W$ if the density of doped particles $n > n^*$, where $n^* = (2/\pi W)\sqrt{|m|(M + |m|)}$. At a lower density, $n < n^*$, the point κ_{c2} is located at smaller values of κ : $(M - |m|)/2 < \kappa < (M + |m|)/2$, with $p_2 \rightarrow 0$ as $\kappa \rightarrow \kappa_{c2} - 0$.

As shown in Fig.10c, in the 4FP-2 phase the four Fermi points $\pm k_{F1}$ and $\pm k_{F2}$ are all located in the upper band $E^+(k)$ and are subject to the condition $k_{F1}^+ + (\pi - k_{F2}^+) = \pi n$. They can be parametrized as $k_{F1} = \pi n - p_2$, $k_{F2} = \pi - p_2$ ($0 < p_2 \ll 1$). At

the transition ($\kappa = \kappa_{c2}$) $p_2 = 0$. Following the same procedure as before we obtain

$$p_2 = \frac{(\pi n)|m|}{A(Q_M - |m|)} \left[\sqrt{1 + (\zeta/\zeta_2)} - 1 \right], \quad (49)$$

$$\zeta_2 = \frac{|m|(\pi n W)^2}{2A Q_M (Q_M - |m|)^2}$$

where $\zeta_2 = (\kappa_{c2} - \kappa)/\kappa_{c2} > 0$ ($\zeta_2 \ll 1$).

Further decreasing κ in the 4FP-2 phase one passes to the region $\kappa < (M - |m|)/2$. The spectrum is shown in Fig.11a. The Fermi momenta k_{F1} and k_{F2} are parametrized as $k_{F1} = p_1$, $\pi - k_{F2} = \pi n - p_1$. p_1 and μ are determined by the equations

$$\sqrt{p_1^2 v_F^2 + M^2} = \mu + \kappa,$$

$$\sqrt{(\pi n - p_1)^2 v_F^2 + m^2} = \mu - \kappa \quad (50)$$

There exists the third Lifshitz transition at $\kappa = \kappa_{c3}$ at which $\mu = E^+(0)$, $p_1 = 0$; see Fig.11b. We find that $\kappa_{c3} = (M - Q_m)/2$, $\mu_{c3} = (M + Q_m)/2$. The requirement $\kappa_{c3} > 0$ is ensured by the condition (31) which sets the upper limit for n . From Eqs.(50) one obtains the quadratic equation valid at $\kappa > \kappa_{c3}$:

$$\left[1 - \frac{(\pi n)^2 W^2}{4\kappa^2} \right] (p_1 v_F)^2 - (\pi n W) \left(1 + \frac{\mu_{c3} \kappa_{c3}}{\kappa^2} \right) (p_1 v_F) + \left(\frac{\mu_{c3}^2}{\kappa^2} - 1 \right) (\kappa^2 - \kappa_{c3}^2) = 0 \quad (51)$$

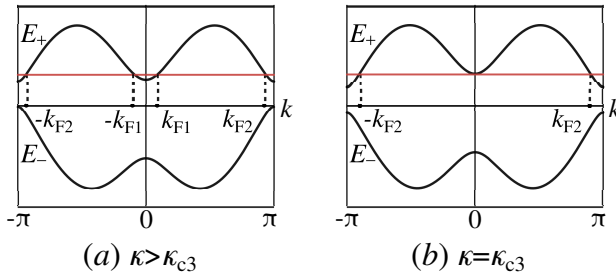
Contrary to all previous cases, a physically acceptable solution of Eq.(51) only exists if $\pi n W > 2\kappa$. This brings the allowed doped particle density n to the interval

$$\frac{M^2 - m^2}{2MW} < \pi n < \frac{\sqrt{M^2 - m^2}}{W} \quad (52)$$

Taking the limit $M \gg |m|$, one then concludes that the transition at $\kappa = \kappa_{c3}$ and the onset of the 2FP-2 phase is only possible at $n \sim M/W$. Choosing $|1 - (\pi n W)^2/\kappa_{c3}^2| \sim 1$, $Q_m \gtrsim M$, $\pi n W \sim M$ we find that

$$p_1(\zeta_3) \sim \sqrt{\zeta_0 + \zeta_3} - \sqrt{\zeta_0}, \quad \zeta_0 \sim \frac{(\pi n)^2 W^2 M}{(M - Q_m)^2 Q_m} \quad (53)$$

where $\zeta_3 = (\kappa - \kappa_{c3})/\kappa_{c3}$. Since $\zeta_0 \sim 1$, only the linear dependence of the momentum p_1 on ζ_3 at $\zeta_3 \ll 1$ is realized. There is no crossover to a square-root asymptotics in this case.

FIG. 11: Lifshitz transition from 4FP-2 to 2FP-2 at $\rho > 1$.

Thus, contrary to the case $\rho < 1$ in which only one Lifshitz transition takes place, at $\rho > 1$ and $m \neq 0$, on increasing the flux towards the value $1/2$ (decreasing κ towards zero) the spectrum of the system undergoes three consecutive Lifshitz transitions

$$\begin{aligned} \kappa = \kappa_{c1} : & \quad 4\text{FP-1 metal} \rightarrow 2\text{FP-1 metal} \\ \kappa = \kappa_{c2} : & \quad 2\text{FP-1 metal} \rightarrow 4\text{FP-2 metal} \\ \kappa = \kappa_{c3} : & \quad 4\text{FP-2 metal} \rightarrow 2\text{FP-2 metal} \end{aligned}$$

where $\kappa_{c1} > \kappa_{c2} > \kappa_{c3}$. In the vicinity of each transition, the behavior of the orbital current at $\rho > 1$ is similar to the already considered case $\rho < 1$.

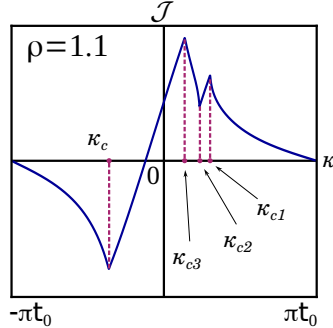
FIG. 12: Cusps in the flux dependence of the orbital current at $\rho > 1$.

Fig.12 shows the flux dependence of the orbital current of a particle-doped ladder ($\rho > 1$) for both signs of $\kappa = 2\pi t_0(1/2 - f)$. Note that due to the symmetry property (23), in Fig.12 the region $\kappa < 0$ with $\rho = 1.1$ can be mapped to the region $\kappa > 0$ with $\rho = 0.9$. Therefore Fig.12 actually demonstrates the clear asymmetry in the flux dependence of the current for particle and hole doped samples (three Lifshitz transitions versus one).

In the 2FP-2 metallic phase the Fermi momentum k_{F2}^+ is fixed by the condition $k_{F2}^+ = \pi(1 - n)$. The

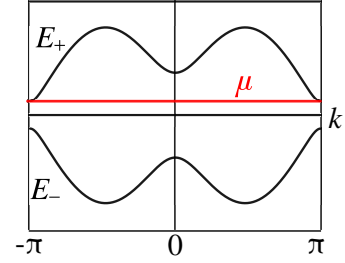
chemical potential is given by $\mu = \kappa + \sqrt{(\pi n)^2 + m^2}$. At $n \rightarrow 0^+$, $\rho \rightarrow 1^+$, the band $E^+(k)$ becomes empty with the chemical potential attached to its bottom:

$$\lim_{n \rightarrow 0} \mu(\kappa) = \kappa + |m| \quad (54)$$

Comparing Figs.9a and 13, and formulas (39) and (54), respectively, we observe that at $\rho \rightarrow 1$ the chemical potential displays a discontinuity :

$$\mu_{\pm}(\kappa) \equiv \lim_{\rho \rightarrow 1^{\pm}} \mu(\kappa) = \kappa \pm |m| \quad (55)$$

Since the classic paper by Lieb and Wu [40] this fact is regarded as a direct manifestation of the insulating nature of the ground state of a system. In fact, for a system with given particle number N with the ground state energy $E_0(N)$, the chemical potentials μ_{\pm} are defined as $\mu_+ = E_0(N+1) - E_0(N)$ and $\mu_- = E_0(N) - E_0(N-1)$. The finite difference $\mu_+ - \mu_- = 2|m| > 0$ then defines the spectral gap of the insulating state.

FIG. 13: $\rho \rightarrow 1^+$, $m \neq 0$

We complete the discussion by noting that the limit $\rho \rightarrow 1$ is unambiguous when the $k \sim \pi$ fermions are massless: $m = 0$. In this case the ground state of the system is always metallic, characterised by a single Dirac point in the spectrum.

VI. CONCLUSION AND OUTLOOK

In this paper we have shown that a noninteracting model of spinless fermions on an asymmetric triangular ladder exhibits interesting properties originating from the interplay of geometrical frustration of the lattice and the external magnetic flux. The main results of our study is applicable to a broader class of frustrated ladders which can be unified into asymmetric Creutz model depicted in Fig.2, the TFL being

the most frustrated member of this family. Contrary to the standard (rectangular) ladder, in a TFL the $k \rightarrow \pi - k$ particle-hole symmetry of the two-band spectrum is absent. At a weak interchain hopping qualitative differences between the two systems become evident when the flux per the diatomic plaquette is close to flux quantum. In this regime, the removal of the double degeneracy of the spectral gap leads to the appearance of two groups of low-energy Dirac-like excitations with different masses. Even for a nearly half-filled spectrum this leads not to a single metal-insulator transition as in the standard ladder, but to a cascade of flux-induced Lifshitz transitions that separate phases with the number of Fermi points equal to 4, 2, 1 or 0, the latter case corresponding to the band insulator phase. The transitions take place when the flux is varied. At the critical points the orbital current and its derivative, the charge stiffness, display singular behavior: universal square-root singularities of the "commensurate-incommensurate" transition type when the chemical potential μ is constant, or cusps when a system is considered at a fixed particle density ρ . We have shown that the TFL displays a generic property that follows from the absence of $k \rightarrow \pi - k$ particle-hole symmetry— different patterns of Lifshitz transitions at a particle ($\rho > 1$) and hole ($\rho < 1$) doping.

Remarkably, for a translationally invariant TFL ($m = t_1 - t_2 = 0$) and the flux close to the value $f = 1/2$, the excitations close to the Brillouin zone boundary ($k = \pi$) become gapless and, in the low-energy limit, transform to a massless Dirac fermion. Such system is very susceptible to interparticle correlations. At sufficiently weak interaction the semi-metallic phase of the TFL will transform to a Tomonaga-Luttinger liquid. However, on increasing interaction one expects the onset of strongly correlated phases formed due to the two-particle interchain processes that become relevant in the renormalization-group sense. As long as the mass gap $|m_s|$ dynamically generated in the strong-coupling phase of the interacting massless model is much smaller than $|m|$, the single-particle branch of excitations still remains well defined up small renormalizations of the mass m and velocity v_F caused by interactions. With such renormalizations taken into account, the results ob-

tained in the present work are applicable to the interacting case as well. As in the non-interacting case, the ground state of the model would be characterized by an explicitly broken parity ($x \rightarrow -x$) with patterns of dimerization of the zigzag bonds depending on the sign of m . The most interesting regime is expected to take place in the range of parameters when the two masses, m_s and m , become of the same order. These and related issues will be addressed in a separate forthcoming publication [28].

From the theoretical point of view, the solution of the two-leg TFL is expected to represent a building block for solving frustrated flux-ladders with a larger number of chains. It is very interesting to formulate a field-theoretical approach to study non-perturbative effects in a weakly coupled multi-chain ladders using methods of Abelian and non-Abelian bosonization [38]. A very different and complicated is the problem of frustrated ladders with a staggered flux. Here one faces a completely different physics already at the level of non-interacting fermions. One of the most challenging issues here is a chiral asymmetry of the spectrum and breakdown of Lorentz invariance.

Recent advances in experimental realization of a Creutz flux ladder for ultracold fermionic atoms in a resonantly driven 1D optical lattice [41] make us believe that the results obtained in the present paper admit their experimental verification.

After completion of this paper we become aware of the recent work [42] in which a bosonic two-chain triangular ladder in the presence of an artificial flux is considered. Even though the physics of bosonic and fermionic flux ladders is quite different, the two systems share the important common feature – the enhanced role of geometrical frustration of the underlying lattice at the values of the flux close to a flux quantum per elementary plaquette.

Acknowledgements

We thank Marcello Dalmonte for reading the manuscript and making a number of important suggestions. We thank him, Titas Chanda, Pierre Fromholz, Emanuele Tirrito and Mikheil Tsitsishvili for fruitful discussions and cooperation in related projects. We are also grateful to George Japaridze and Oleg Starykh for interesting conversations on the

effects of frustration in one-dimensional quantum systems. The authors acknowledge the support from the Shota Rustaveli National Science Foundation of Georgia, SRNSF, Grant No. FR-19-11872.

gia, SRNSF, Grant No. FR-19-11872.

-
- [1] L.D. Landau and E.M. Lifshitz, *Quantum Mechanics*, 3rd ed. (Pergamon, Oxford, 1977).
 - [2] R.E. Peierls, *Z.Phys.* **80**, 763 (1933).
 - [3] L. Onsager, *Philos. Mag.* **43**, 1006 (1952).
 - [4] Q. H. Wannier, *Rev. Mod. Phys.* **34**, 645 (1962).
 - [5] P. G. Harper, *Proc. Phys. Soc. London* **68**, 874 (1955).
 - [6] M. Ya Azbel', *Zh. Eksp. Teor. Fiz.* **46**, 929 (1964) [*Sov. Phys. JETP* **19**, 634 (1964)].
 - [7] E. Brown, *Phys. Rev.* **133**, A1038 (1964).
 - [8] R. Hofstadter, *Phys. Rev. B* **14**, 2239 (1976).
 - [9] Y. Hasegawa, P. Lederer, T. M. Rice, and P. B. Wiegmann, *Phys. Rev. Lett.* **63**, 907 (1989).
 - [10] W. Barford and J.H. Kim, *Phys. Rev. B* **43**, 559 (1991).
 - [11] J. Dalibard, F. Gerbier, G. Juzeliūnas, and P. Ölborg, *Rev. Mod. Phys.* **83**, 1523 (2011).
 - [12] A. Celi, P. Massignan, J. Ruseckas, N. Goldman, I.B. Spielman, G. Juzeliūnas, and M. Lewenstein, *Phys. Rev. Lett.* **112**, 043001 (2014).
 - [13] V. Galitski, G. Juzeliūnas, and I. Spielman, *Physics Today* **72**, 39 (2019).
 - [14] E. Orignac, and T. Giamarchi, *Phys. Rev. B* **64**, 144515 (2001).
 - [15] H. Miyake, G. A. Siviloglou, C. J. Kennedy, W. C. Burton, and W. Ketterle, *Phys. Rev. Lett.* **111**, 185302 (2013).
 - [16] M. Atala, M. Aidelsburger, M. Lohse, J. T. Barreiro, B. Paredes, I. Bloch, *Nature Physics* **10**, 588 (2014).
 - [17] L.F. Livi, G. Cappellini, M. Diem, L. Franchi, C. Clivati, M. Frittelli, F. Levi, D. Calonico, J. Catani, M. Inguscio, and L. Fallani *Phys. Rev. Lett.* **117**, 220401 (2016).
 - [18] B.N. Narozhny, S.T. Carr, and A.A. Nersesyan, *Phys. Rev. B* **71**, 161101(R) (2005).
 - [19] S.T. Carr, B.N. Narozhny, and A.A. Nersesyan, *Phys. Rev. B* **73**, 195114 (2006).
 - [20] J. C. Budich, A. Elben, M. Lacki, A. Sterdyniak, M. A. Baranov, and P. Zoller, *Phys. Rev. A* **95**, 043632 (2017).
 - [21] S. Barbarino, L. Taddia, D. Rossino, L. Mazza, and R. Fazio, *New J. Phys.* **18**, 035010 (2016).
 - [22] S. Barbarino, M. Dalmonte, R. Fazio, and G. Santoro, *Phys. Rev. A* **97**, 013634 (2018).
 - [23] M. C. Strinati, E. Cornfeld, D. Rossini, S. Barbarino, M. Dalmonte, R. Fazio, E. Sela, and L. Mazza, *Phys. Rev. X* **7**, 021033 (2017).
 - [24] C-H. Huang, M. Tezuka, and M. A. Cazalilla, *New J. Phys.* **24**, 033043 (2022).
 - [25] A. Mazurenko, C. S. Chiu, G. Ji, M. F. Parsons, M. Kanász-Nagy, R. Schmidt, F. Grusdt, E. Demler, D. Greif, and M. Greiner; *Nature*, **545**, 462 (2017).
 - [26] S. Krinner, T. Esslinger and J.-P. Brantut. *J. Phys.: Condens. Matter* **29**343003 (2017).
 - [27] L. Lepori, A. Maraga, A. Celi, L. Dell'Anna and A. Trombettoni, *Condens. Matter* **3**, 14 (2018).
 - [28] B. Beradze, T. Chanda, E. Tirrito, M. Tsitsishvili, M. Dalmonte and A. Nersesyan (in preparation).
 - [29] M. Creutz, *Phys. Rev. Lett.* **83**, 2636 (1999).
 - [30] A. Y. Kitaev *Phys.-Usp.* **44**, 131 (2001).
 - [31] J. Alicea, *Rep. Prog. Phys.* **75**, 076501 (2012).
 - [32] A.W.W. Ludwig, *Phys. Scr.* **T168**, 014001 (2016).
 - [33] G.E. Volovik, *Low Temperature Physics*, **43**, 47 (2017); arXiv:1701.06435, cond-mat, 2017.
 - [34] G. I. Japaridze and A. A. Nersesyan, *Pisma Zh. Eksp. Teor. Fiz.* **27**, 356 (1978) [*Sov. Phys. JETP Lett.* **27**, 334 (1978)].
 - [35] V. L. Pokrovsky and A. L. Talapov, *Phys. Rev. Lett.* **42**, 65 (1979).
 - [36] B.S. Shastri and B. Sutherland, *Phys. Rev. Lett.* **65**, 243 (1990).
 - [37] T. Giamarchi and B.S. Shastri, *Phys. Rev. B* **51**, 10915 (1995).
 - [38] A. O. Gogolin, A. A. Nersesyan, and A. M. Tsvelik, *Bosonization and Strongly Correlated Systems*, Cambridge University Press, Cambridge, 1998.
 - [39] T. Vekua, *Phys. Rev. B* **80**, 104411 (2009).
 - [40] E.H. Lieb and F.Y. Wu, *Phys. Rev. Lett.* **20**, 1445 (1968).
 - [41] J. H. Kang, J. H. Hun, and Y. Shin, *New J. Phys.* **22**, 013023 (2020).
 - [42] C.-M. Halati, T. Giamarchi, arXiv: 2210.14594, cond-mat. (2022)
 - [43] In fact, the location of the lowest-energy states close to the zone boundary $k = \pi$ is a robust property of the model valid as long as $|t_1 - t_2| \ll |t_1 + t_2|$ irrespective of the magnitude of the ratios $t_{1,2}/t_0$. On the other hand, a local minimum of E_k at $k = 0$ only exists under the condition $t_1 t_2 < 4t_0^2$; otherwise E_k has a local maximum at $k = 0$.